Deutscher Luft- und Raumfahrtkongress 2022
DocumentID: 570075

EXPERIMENTAL WIND TUNNEL RESULTS FOR RADIATION OF SOUND FROM SEMI-BURIED DUCTS

M. Mößner*, J.-W. Delfs*, M. Pott-Pollenske*
* German Aerospace Center, Technical Acoustics, Lilienthalplatz 7, Braunschweig, Germany

Abstract

Semi-buried engines are part of of many future aircraft designs. From acoustic's point of view the increased noise shielding is one of the potential benefits. But at the same time the fan will experience a disturbed inflow which can lead to additional noise. In order to assess such new concepts numerical predictions can help, but it at the same time it is important to validate the methods against experimental data. The current paper describes a wind tunnel experiment which can serve as a validation case. The setup consists of a duct which is mounted on a flat plate. The whole model is placed inside a wind tunnel and tested with different flow speeds. Upstream the duct, a boundary layer develops which enters the duct, imitating boundary layer ingestion. The sound is generated by a specially designed source that it can be easily translated to computational methods. All important design details are given which makes it possible to use it as a benchmark case for numerical methods.

The sound radiation is measured upstream the duct. Since the sound source operates at dedicated frequencies, clear interference patterns become visible. Such patterns can help to make small configuration changes visible (e.g. different flow speeds). The results serve as a starting point for detailed studies of flow and boundary layer effects on sound radiation from a duct. Numerical methods can be validated against the given result and extend the parameter range e.g. to much thicker boundary layers as well as recording results at much larger evaluation planes. However, such numerical studies are beyond the scope of this paper.

Keywords

BLI; wind tunnel experiments; sound radiation

1. INTRODUCTION

The trend to larger engines like ultra high bypass ratio (UHBR) engines raises the question for the benefits and drawbacks of highly integrated engines. From perspective of engine noise, one benefit is the potentially better noise shielding. However, if a boundary layer enters the engine it will hit the fan (figure 1), and if this is not rotation symmetric it will cause additional noise. Also, part of the sound waves, which are leaving the nacelle, move along the boundary layers and, thus, undergo refraction effects (figure 2). For a 2D case, these effects were shown to be small, [1], but it would be interesting to get more insights for a fully involved 3D case. Ideally, numerical prediction tools can help to quantify the different effects, but it is important to have a database to prove the validity of the results.

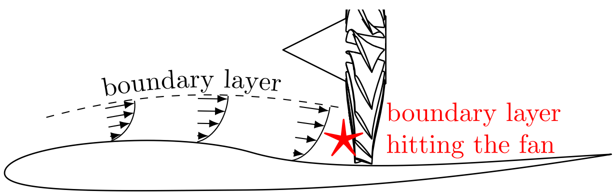

FIG 1. Boundary layer hitting the engine fan.

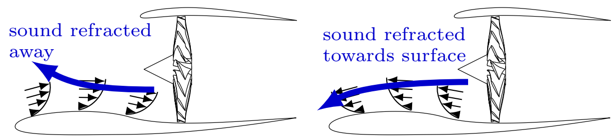

FIG 2. Refraction of sound waves in boundary layer.

This paper presents an experiment with the focus on sound propagation from of a semi-buried duct. The experiment is designed such that the sound source can be easily reproduced while placing the main focus on sound propagation. The influence of major parameter changes like the flow speed in and around the duct as well as the duct geometry itself is studied. Triggering dedicated frequencies leads to interference pattern at the evaluation microphones such that even small radiation changes can clearly be seen.

2. DESIGN OF EXPERIMENT

Figure 3 shows the two wind tunnel model variants used throughout this paper. A round cylinder is integrated on a flat plate. To the left, the tube is placed on top of the plate, and to the right it is buried $30\,\%$ of its diameter into the plate. The dimensions of the tube are drawn in figures 4 and 5. The tube consists

doi: 10.25967/570075

of two segments, the 1.9 m long downstream segment has a round cross section and the 2 m long upstream segment blends from the round segment to the inlet region. Pressure taps are placed along the bottom of the blending segment. 0.76 m in front of the channel, a microphone traverse can move up and down to capture the sound which is radiated from the tube. The channels are open-ended, but in order to avoid reflecting sound waves, an inlay is placed at the channel end following the work of Shenoda [2].

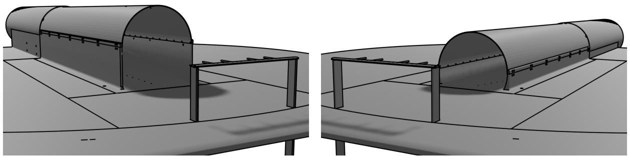

FIG 3. Render view of wind tunnel models. Left hand side: $0\,\%$ buried, right hand side: $30\,\%$ buried.

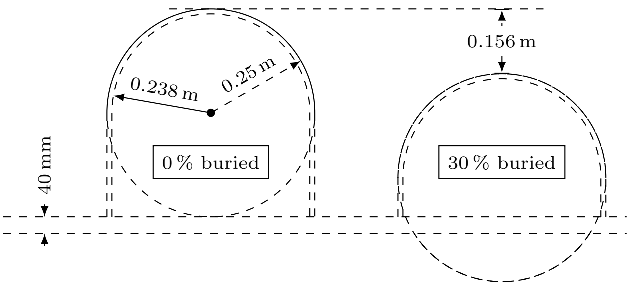

FIG 4. Front view dimensions for the two wind tunnel model variants.

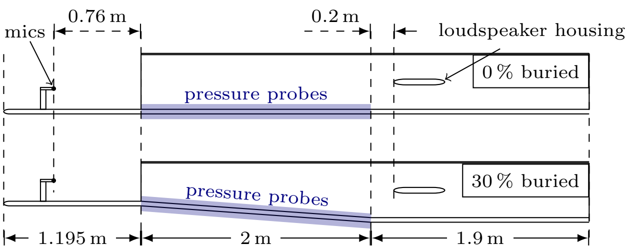

FIG 5. Side view dimensions of the two wind tunnel model variants.

Sound is generated within the channel by a loudspeaker inside a housing which is centered radially within the round segment of the cylinder. The housing is shown in detail in figure 6. Close to the front, there are 36 slits placed equidistantly over the circumference. Each slit is 2 mm wide and 20 mm long. Inside the housing there is a loudspeaker, which radiates against a wave guide to deflect the sound outwards though the slits. The setup is sketched in figure 7. The whole speaker setup is designed to be unaffected from the flow around the housing. Having the slits sideways means that the loudspeaker will only experience static pressure changes, but not be affected by the high dynamic pressure within stagnation areas.
The main flow effects which are expected to be seen at the microphone traverse are

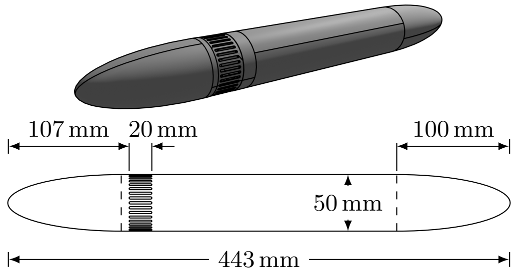

FIG 6. Speaker housing.

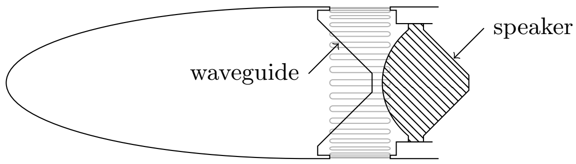

FIG 7. Loudspeaker positioning within the housing.

1) Convection effects
2) Refraction in boundary layers

It would be interesting to have a measuring setup, which can take the two effects apart, but since the utilized wind tunnel is limited to adjusting the flow velocity (and not e.g. the temperature), this is no easy task. Such investigations will be left for numerical investigations, where one can easily vary Mach and Reynolds number independently.
Regarding refraction in boundary layers a rough estimation of the expected dimensions will be given. According to boundary layer theory (see e.g. [3]), the thickness of a turbulent boundary layer on a flat plate can be estimated as

$$\delta \approx 0.376 \frac{x}{Re^{\frac{1}{5}}} \tag{1}$$

For flow speeds around $20\,\frac{\text{m}}{\text{s}}$ to $50\,\frac{\text{m}}{\text{s}}$ and standard ambient conditions, the expected boundary layer thickness at the channel inlet is roughly 20 mm to 30 mm. The expected wave length for the excited frequencies of 3 kHz-6 kHz is in the range of 50 mm-100 mm. Wave lengths much longer than the boundary layer thickness would mean that the expected effects are very small. In the given case, the wave length is about 2-5 times longer than the boundary layer thickness plus the waves are traveling a long way along the walls, so we can expect, that refraction effects are small but not negligible.

3. WIND TUNNEL INSTALLATION

The model is installed within the low-speed atmospheric wind tunnel DNW-NWB in DLR Braunschweig. This is a facility of Göttingen design with a closed loop and equipped with low-noise technology. An open test section was used which allows suppressing most of acoustic reflections. The duct size is $\sim 3.25\,\text{m} \times 2.8\,\text{m}$. Flow speeds up to $80\,\frac{\text{m}}{\text{s}}$ are possible, but for the current experiment the speeds were set in-between $0\,\frac{\text{m}}{\text{s}}$ and $50\,\frac{\text{m}}{\text{s}}$.

4. FLOW RESULTS

Very basic flow measurements were conducted in order to make numerical validation of the whole setup possible. As indicated previously, pressure probes were installed within the front part on the channel which measure the static pressure along the center-line of the channel bottom. The results for both channels, $0\,\%$ buried and $30\,\%$ buried, are shown in figure 8.

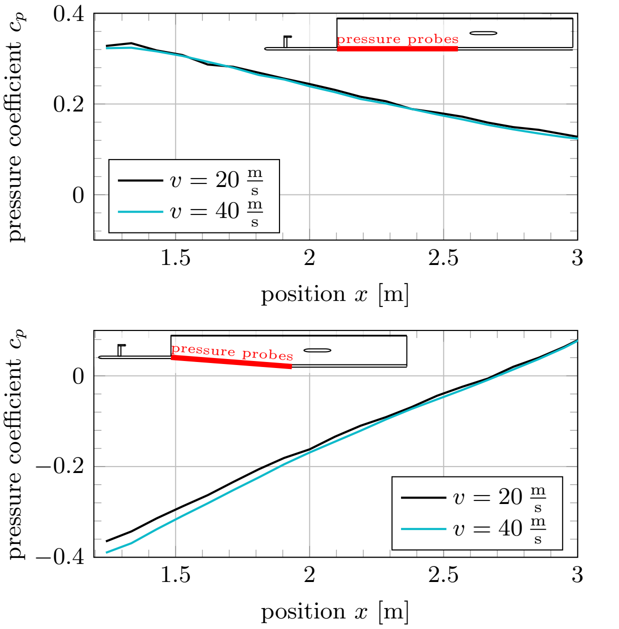

FIG 8. Pressure coefficient c_p along the blending channel region from the channel inlet down to the circular cross section for the $0\,\%$ buried channel (top) and the $30\,\%$ buried channel (bottom).

For all measured flow velocities (only 2 results are shown, but more have been measured), the distribution of the pressure coefficient c_p is very similar, indicating, that the Reynolds number effects are rather small. This is consistent with the fact, that the expected boundary layer thicknesses of less than $30\,\mathrm{mm}$ are small compared to the channel inlet dimensions of $\sim 500\,\mathrm{mm}$.

The $0\,\%$ buried channel shows a drop of pressure along the channel since the effective flow area decreases with the axial position x: At the most upstream pressure measurement, the channel is merged with the wall, so its cross section area is larger than the position of the most downstream measurement where the cross section is fully round. In contrast, the $30\,\%$ buried channel has an increasing cross section area as the flow moves downstream. As a result, a pressure rise can be observed.

In dedicated measurement runs, a pressure rake was installed in front of the $30\,\%$ buried channel in order to measure the boundary layer. Two positions were measured, $315\,\mathrm{mm}$ behind the plate leading edge, which corresponds to $88\,\mathrm{mm}$ upstream the channel inlet and $862\,\mathrm{mm}$ behind the plate leading edge, which corresponds to $333\,\mathrm{mm}$ upstream the channel inlet. The pressure coefficients c_p are plotted in figure 9. The plots show the expected trends that the boundary layer thicknesses grow with decreasing flow velocities. Both, the measurement results and equation (1), yield similar boundary thicknesses of $\delta \sim 10\,\mathrm{mm}$ at $x = 315\,\mathrm{mm}$ and $\delta \sim 20\,\mathrm{mm}$ at $x = 862\,\mathrm{mm}$.

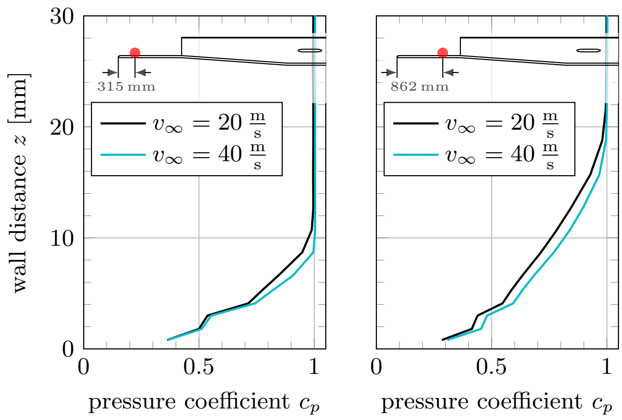

FIG 9. Pressure coefficient c_p at two pressure rakes for boundary layer measurements.

In summary, all flow measurements yield consistent results. In terms of acoustics, the boundary layers lead to refraction effects, so it is important to know the rough thicknesses for later evaluations. Also, if the results are used as validation case for numerical simulations, it will be important to show that the flow is predicted correctly.

5. RADIATION CHARACTERISTICS OF ISOLATED SOURCE

The design of the sound source, a speaker within a housing, is already described in section 2. Before installing the source inside the channels, the source was mounted inside an anechoic room in order to measure its radiation characteristics and also to find loudness calibration factors. The setup is sketched in figure 10, showing the two lines parallel to the source center-line which were traversed.

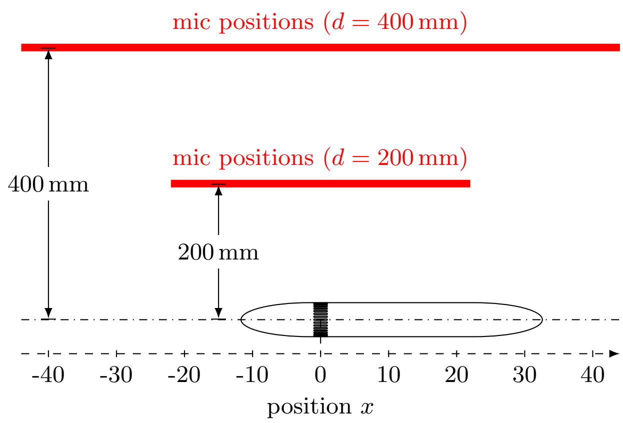

FIG 10. Microphone positions for measuring the emitted sound of the isolated source.

Figure 11 shows the sound pressure levels (SPL) for the two traversed lines for different frequencies. All results are based on a speaker input power of $2\,\mathrm{W}$[1]. For each frequency the line was traversed separately, in order to provide a clear relation between input power and sound pressure level.

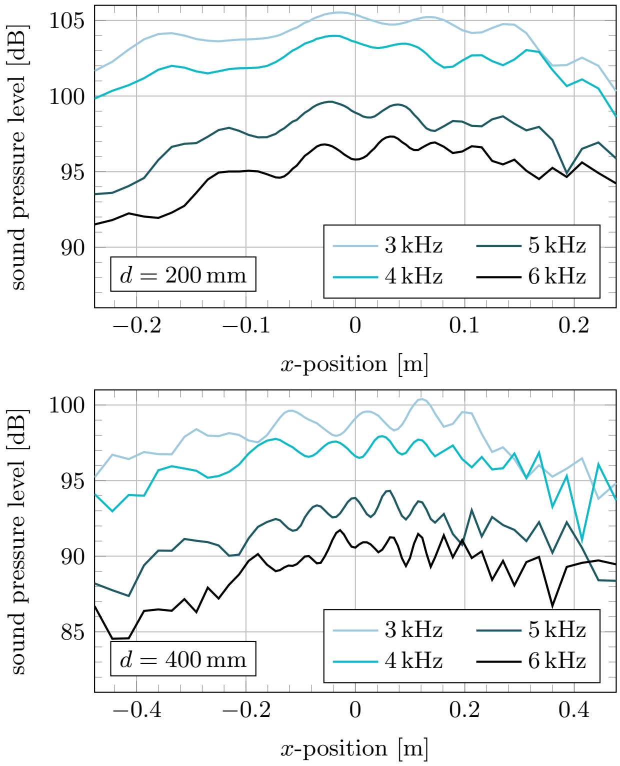

FIG 11. Sound pressure level of isolated sound source along two traversed lines parallel to the speaker housing.

The results show that there is a significant interference pattern in form of a wavy pattern for all frequency lines, which is no surprise for single-frequency measurements. Apart from the wavy pattern, it can be observed that the efficiency of the speaker is decreasing with increasing frequencies. The peak SPL values are close to position $x = 0$, which is expected since it is closest to the slits of the housing. Comparing the lines at different distances $d = 200\,\mathrm{mm}$ and $d = 400\,\mathrm{mm}$ the sound pressure level is $\sim 6\,\mathrm{dB}$ lower for the $400\,\mathrm{mm}$ line. This the expected value for a monopole source in 3D where the pressure amplitude decreases with the inverse of the distance.

6. ACOUSTIC RESULTS

As outlined before, the two different channel setups were installed in the DNW-NWB wind tunnel and the emitted sound was measured $0.76\,\mathrm{m}$ upstream the channel inlet. The microphone traverse contained 8 microphones next to each other placed symmetrically around the channel symmetry plane, as shown in figure 12. The microphones were traversed starting from the plate surface up to a distance from the plate of about $\sim 0.5\,\mathrm{m}$. This allows to show the sound pressure levels on a plane in front of the channel as sketched in figure 13. The different frequencies were measured separately with an input power of $2\,\mathrm{W}$ each.

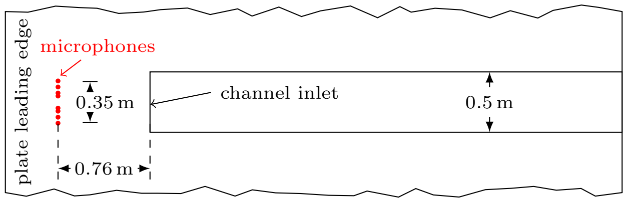

FIG 12. Positions of microphones in front of the channels.

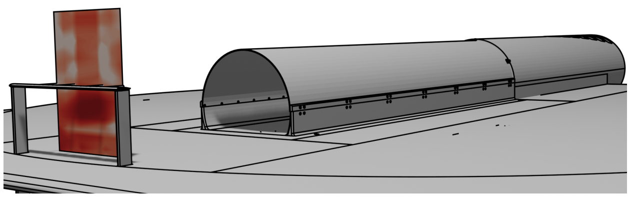

FIG 13. Position of evaluation plane for noise measurements in front of the channel.

Figure 14 shows the frequency-dependent sound pressure level at different frequencies for a wind tunnel flow velocity of $v = 40\,\frac{\mathrm{m}}{\mathrm{s}}$. The top row contains the results of the $0\,\%$ buried channel, the bottom row the results of the $30\,\%$ buried channel. The resulting patterns are dominated by interference effects. Depending on the frequencies the locations of quiet and loud areas completely differ, for higher frequencies the patterns become more fine-grained. For the present case of tonal noise such a dependency is not surprising and is a very good candidate for validation numerical results since small errors can lead to large deviations of the results.

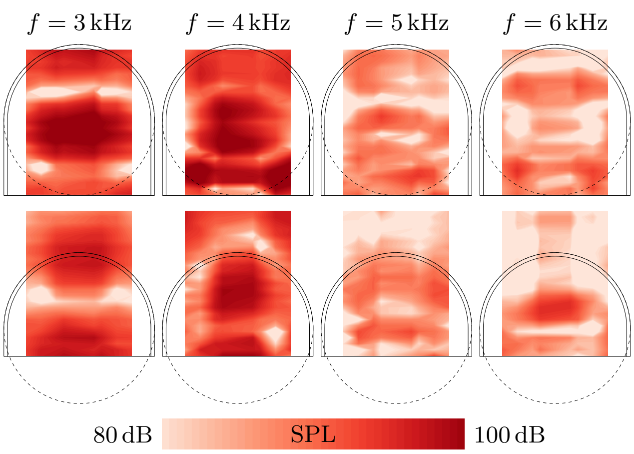

FIG 14. Contour plots for different frequencies at a wind tunnel speed of $v = 40\,\frac{\mathrm{m}}{\mathrm{s}}$. Top row: $0\,\%$ buried, bottom row: $30\,\%$ buried.

[1] It should be mentioned, that the actual measurements took place at input power of $0.5\,\mathrm{W}$ to not overly stress the ears, but all results are then carefully scaled to $2\,\mathrm{W}$ input power by some extra calibration measurements to match the later measurements with the channel.

The effect of different wind tunnel velocities is shown in figure 15 which plots the center-line data (which means averaging the data at $y = \pm 0.05\,\mathrm{m}$ which are the microphones closest to the center-line $y = 0$). For both configurations, $0\,\%$ buried and $30\,\%$ buried, the effect of flow speed is small. Still, there appears to be a small systematic shift with increasing velocities. There are three potential candidates which could explain the differences:

1) Increasing background noise with higher wind tunnel flow speeds.
2) Refraction effects in the boundary layer.
3) Convection effects leading to altered interference patterns.

It can be expected that increased background noise due to flow speeds is not the main source of the differences since at certain points also a reduction of noise can be observed with higher flow speeds. Also, the data is filtered, such that additional broadband noise at other frequencies than the speaker frequency does not increase the noise levels.

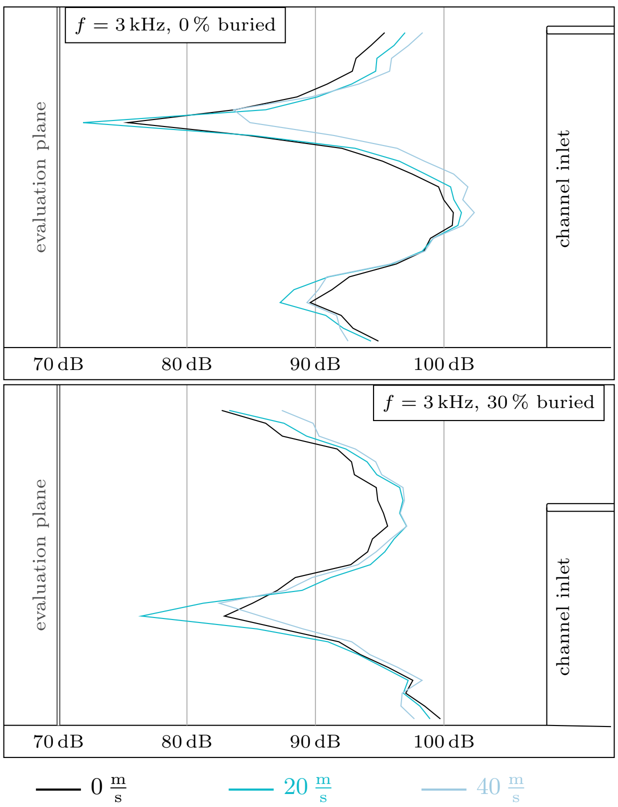

FIG 15. Averaged SPL levels of microphones closest to center ($y = \pm 0.05\,\mathrm{m}$) at a frequency of $3\,\mathrm{kHz}$ and different wind tunnel speeds.

Refraction effects would be desirable especially for noise shielding applications, since sound energy can be systematically deflected away from the observer. One would expect to see an effect especially close to the wall. Indeed, this is the case when looking at the very first data point above the wall. With higher flow velocities, the sound pressure levels seem to decrease. However, with the limited amount of data, it is difficult to make definite statements here. Also, with increasing flow speed the boundary layer thickness will decrease and at some point it will be too thin to have a significant refraction effect. Numerical simulations are needed to give more insight here.

Most presumably, the dominant effect caused by the flow velocity is a shift of interference patterns. A hint which supports this theory is that the lines are not just shifted but change shape. But also here, it is difficult to give a definite answer.

For sake of completeness, additional plots are shown for the $0\,\%$ embedded channel at higher frequencies for flow velocities of $v = 0\,\frac{\mathrm{m}}{\mathrm{s}}$ and $v = 40\,\frac{\mathrm{m}}{\mathrm{s}}$ in figure 16. Flow effects are clearly visible, but it is difficult to isolate a clear pattern. The previously mentioned observation that there might be refraction effects close to the wall still holds for the frequencies $f = 4\,\mathrm{kHz}$ and $f = 5\,\mathrm{kHz}$, but not for $f = 6\,\mathrm{kHz}$ if looking at the first 2 data points next to the wall. As said, more data is needed for better interpretations. With increasing frequency, the $v = 0\,\frac{\mathrm{m}}{\mathrm{s}}$ and $v = 40\,\frac{\mathrm{m}}{\mathrm{s}}$ lines deviate more and more from each other also in shape, which is obvious since the interference patterns are more fine-grained. It is unknown though, if the change of interference patterns is dominated by convection effects or boundary layer refraction.

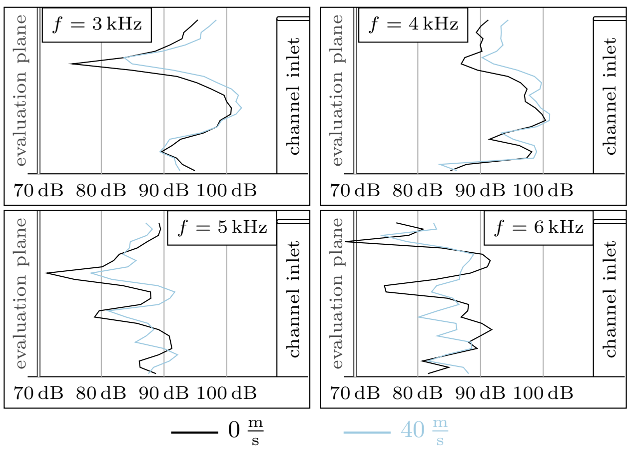

FIG 16. Averaged SPL levels of microphones closest to center ($y = \pm 0.05\,\mathrm{m}$) at different frequencies and wind tunnel speeds for the $0\,\%$ buried channel.

7. SIMULATIONS

While this paper mainly focuses on showing experimental results, simulation results of the setup are shown in the following. On the one hand this supports the validity of the experiments, and on the other hand it helps to give a rough understanding of the underlying uncertainties.

Figure 17 shows the pressure coefficient of the two different channels at a wind tunnel velocity of $v = 40\,\frac{\mathrm{m}}{\mathrm{s}}$. The results were obtained with the solver DLR TAU-Code [4], and the underlying turbulence model was a Spalart-Allmaras one-equation model. One can nicely see the pressure increase towards the channel inlet of the $0\,\%$ buried channel and the pressure decrease for the $30\,\%$ buried channels.

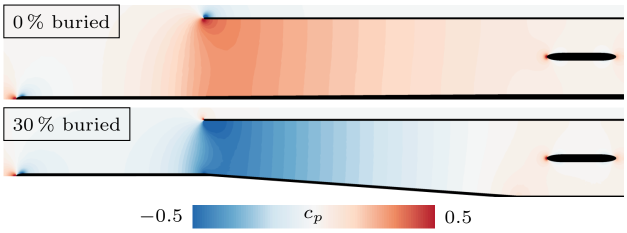

FIG 17. Pressure coefficient c_p at center plane of channels at wind tunnel velocity of $40\,\frac{\mathrm{m}}{\mathrm{s}}$.

A comparison against the experimental data is shown in figure 18. The slope between experiment and CFD result is similar, but for the $30\,\%$ buried channel there is a c_p-offset of almost 0.1 The differences could e.g. origin from higher energy losses of the flow on it's way around the flat plate, such that the pressure at the channel outlet is higher for the experiments. It should be mentioned, that the results at other flow velocities (not shown in this paper) look almost the same and also the differences are very similar.

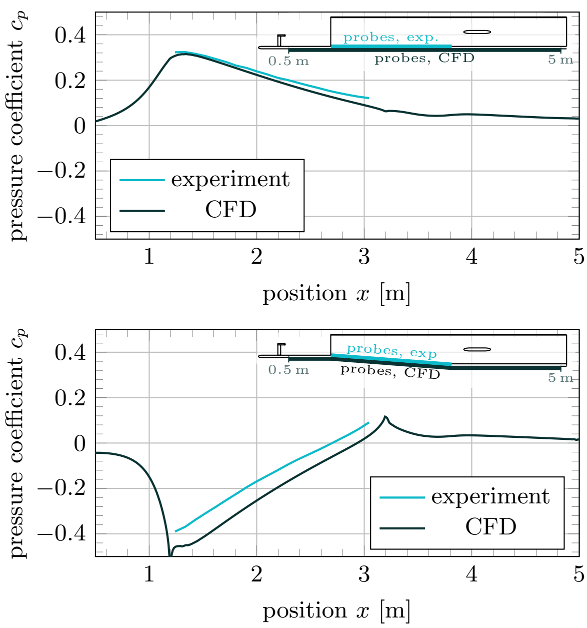

FIG 18. Pressure coefficient c_p along the bottom centerline for the $0\,\%$ and $30\,\%$ buried channels at a wind tunnel velocity of $40\,\frac{\mathrm{m}}{\mathrm{s}}$.

The boundary layers of experimental and CFD results for the $30\,\%$ buried channel case are compared in figure 19. Also here, the results are similar, but the experimental data tends to a bit thicker boundary layers.

In summary, the CFD can show that the flow in the wind tunnel experiments in and around the channel is behaving in a well-defined way. There are differences compared to the CFD but the goal of the flow measurements was not meant to yield highly precise results, but rather to validate that the flow behaves as expected.

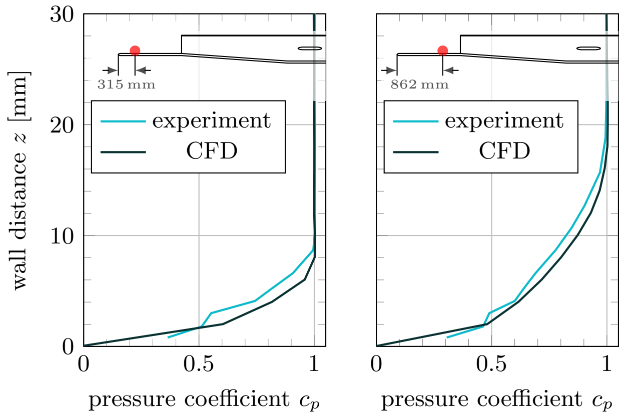

FIG 19. Pressure coefficient c_p at two pressure rakes for boundary layer measurements at a wind tunnel velocity of $40\,\frac{\mathrm{m}}{\mathrm{s}}$.

For the acoustic simulations, the DLR solver DISCO++ [5] was used. This is a 4th discontinuous Galerkin code, solving the acoustic perturbation equations [6]. The sound source was reproduced by closing the slits in the speaker housing and predefining a fluctuating normal velocity at the closed surfaces.

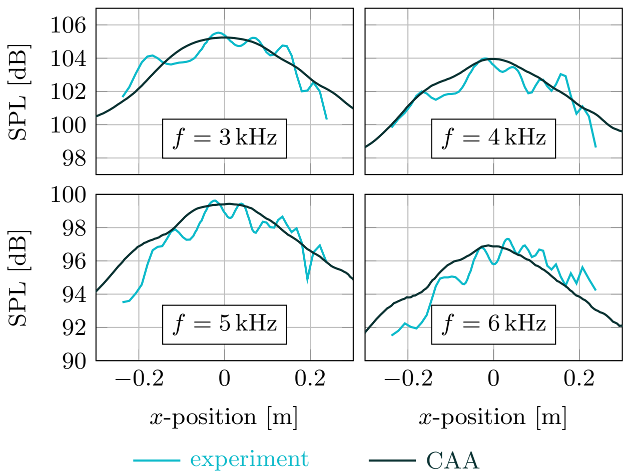

FIG 20. Comparison of sound pressure level for measurements and simulation of the isolated speaker at an axis with $200\,$mm distance to the speaker center-line.

To be able to compare absolute sound pressure levels, the isolated sound source was simulated and compared with the corresponding measurements. The numerical results are scaled to match the experiments as good as possible. The resulting calibration factors are remembered and used for all later comparisons of the channel simulations. Note that the described procedure is only possible, since the acoustic equation systems are linear, meaning that scaling the sound source has no other effect than scaling the results. The directivity results of the isolated sound source are shown in figure 20. For low frequencies, the peak position is nicely met, but for higher frequencies, the results are slightly shifted.

Also the simulation does not show the interference pattern of the measurements. Obviously, the sound propagation inside the housing has some effect here. In the following, an overview of the acoustic simulations of the channel is presented. It will be shown that numerical simulations are able to reproduce the experimental results with good quality for the lower frequencies. But it also becomes clear, that for high frequencies the results are not as reliable. Figure 21 compares the data for the two different channels at two velocities. The interference patterns match very well for all cases. This makes clear, that the numerical methods are capable of resolving the main effects of channel geometry and flow. Without showing an explicit comparison, it should be noted, that also trends with increasing velocity are well reproduced.

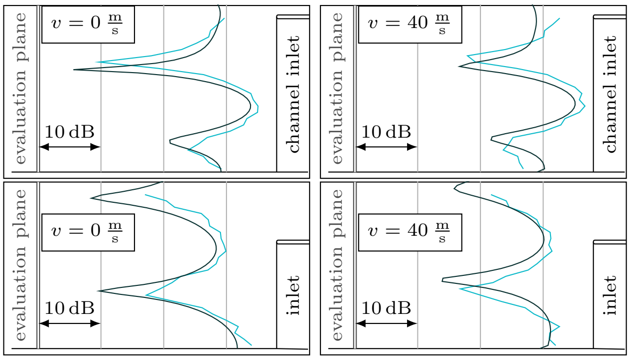

FIG 21. Comparing SPL levels from experiment and simulation at microphones closest to center ($y = \pm 0.05$ m) at $f = 3$ kHz, for different velocities and $0\,\%$ (top row) and $30\,\%$ (bottom row) buried channels.

Also for higher frequencies, the patterns can be reproduced, but the quality is affected. Figure 22 shows the results for the $0\,\%$ buried channel at a wind tunnel speed of $40\,\frac{m}{s}$. The $f = 4$ kHz case shows an underprediction of ~ 5 dB close to the wall, and the interference pattern of the $f = 6$ kHz case only loosely reproduces the patterns. But apart from this, one can say that the experiment and numerics match well.

8. CONCLUSION

A wind tunnel experiment was described to serve as a validation case for flow effects at ducts of semi-buried engines. The intention of the experiment is twofold: Serving as a validation database for numerical methods but also to give insights into the effect of boundary layer ingestion on sound leaving the engine.
Two different channels were tested, one placed on top of a flat plate ($0\,\%$ buried) and one that is buried $30\,\%$ of its diameter into the flat plate. The channel was instrumented with several pressure probes which allows to validate numerical flow simulations. Also the boundary layer thickness was measured for a single test case.

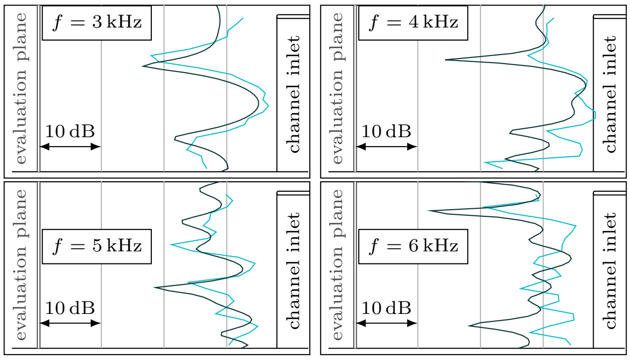

FIG 22. Comparing SPL levels of the $0\,\%$ channel from experiment and simulation at microphones closest to center ($y = \pm 0.05$ m) at $f = 40\,\frac{m}{s}$, for different frequencies.

Sound was generated with a speaker inside housing, which was first measured in isolation. This helps to calibrate the strength of the sound source in numerical simulations. But it also characterizes the directivity of the sound source.
The most important results shown in the paper is the sound radiating from the semi-buried channels. By varying the wind tunnel speed, one would hope to get some insight into the sound interacting with the boundary layers. Unfortunately, this question cannot be answered. The sound pattern in front of the channel is dominated by interference patterns, which are sensitive not only to boundary layers, but also to convection effects. However, it could be shown that numerical methods can well reproduce the results. So in a next step more variations could be run with numerical simulations. One could e.g. vary the fluid viscosity to generate thicker boundary layers at the same flow speed. The given experiments can be seen as the starting point for more involved studies and understandings of the acoustic propagation effects of highly integrated engine ducts.

Contact address:

michael.moessner@dlr.de

References

[1] J. W. Delfs, M. Mößner, and K.-S. Rossignol. Influence of flow on noise shielding. In Andreas Dillmann, Gerd Heller, Ewald Krämer, Claus Wagner, Cameron Tropea, and Suad Jakirlić, editors, *New Results in Numerical and Experimental Fluid Mechanics XII*, pages 729–738. Springer International Publishing, 2020.

[2] F. B. Shenoda. *Reflexionsarme Abschlüsse für durchströmte Kanäle.* phdthesis, Technische Universität Berlin, Berlin, 1973.

[3] I. H. Shames. *Mechanics of Fluids.* McGraw-Hill series in mechanical engineering. McGraw-Hill, 1992.

[4] D. Schwamborn, T. Gerhold, and R. Heinrich. The dlr tau-code: Recent applications in research and industry. In Wesseling p., E. Oñate, and J. Périaux, editors, *European Conference on Computational Fluid Dynamics*. TU Delft, 2006.

[5] M. Lummer. A Hybrid 3D Discontinuous Galerkin Code for CAA Applications. In *22nd AIAA/CEAS Aeroacoustics conference*, number AIAA 2016-2719, Lyon, France, 2016. AIAA.

[6] R. Ewert and W. Schröder. Acoustic perturbation equations based on flow decomposition via source filtering. *Journal of Computational Physics*, 188(2):365–398, 2003.